Earthquake Research Advances 6 (2026) 100393

Contents lists available at ScienceDirect

Earthquake Research Advances

journal homepage: www.keaipublishing.com/en/journals/earthquake-research-advances

Mutual influence mechanism between soft soil interlayers and shield tunnels under seismic action: Laboratory tests and numerical simulations

Xinwei Tang [a], Gaozhi Xin [a], Danqing Song [a,b,*]

[a] State Key Laboratory of Subtropical Building and Urban Science, School of Civil Engineering and Transportation, South China University of Technology, Guangzhou, 510640, China
[b] Nanjing University (Suzhou) High-Tech Institute, Suzhou, 215123, China

ARTICLE INFO

Keywords:
Soft soil interlayers
Shield tunnels
Seismic response
Numerical simulation
Influence mechanism

ABSTRACT

Soft soil is widely distributed and has complex origins. Shield tunnels are inevitably constructed within soft soil interlayers, and under seismic action, tunnels may be subject to severe damages. On the basis of actual engineering, this study utilized dynamic triaxial testing to investigate the dynamic properties of soft soil. Using the PIMY constitutive model, the seismic subsidence characteristics of the soft soil were characterized, and a refined finite element model was established to study the mutual influence mechanism between the soft soil layer and shield tunnels via the open-source software framework OpenSees. The results demonstrate that soil exhibits a softening effect under dynamic loading; soft soil with better structural integrity is less prone to seismic subsidence; and the greater the inertial force acting on the soft soil, the greater the likelihood of settlement. Under seismic action, the presence of the shield tunnel exacerbates the settlement of the soft soil, as the surrounding soil experiences significant inertial forces from the tunnel structure, hindering drainage and accelerating the accumulation of pore water pressure; The soft soil itself has large deformation and displacement under the action of earthquake, which leads to the great stress, deformation, and displacement of the structure. The arch foot position of the tunnel is identified as the most vulnerable to damage.

1. Introduction

The subsequent optimization project of the Hanjiang, Rongjiang, and Lianjiang water systems is a major livelihood water conservancy project. It is also an important part of Guangdong Province's “Five Vertical and Five Horizontal” backbone water resource allocation network. It is of significant importance for solving resource and engineering water shortage problems in the eastern Guangdong region, supporting high-quality economic and social development in Guangdong. Soft soil is widely distributed and has complex origins, including marine, estuarine, river alluvial, and deltaic deposits. Marine soft soil accounts for a large proportion and is a common weak interlayer in coastal areas. For example, Tokyo (Yamashita et al., 2012), HongKong (Tong et al., 2012) and Shanghai (Sun et al., 2019) are distributed. Shield tunnels were planned for construction in certain sections of the project. Shield tunnels have difficulty in crossing through soft soil layers, such as mud, as shown in Fig. 1.

The 2–1 soil layer has a high moisture content, a low blow count of SPT, and relatively soft soil. Soft soil sites are prone to subsidence damage under seismic action (Jara et al., 2023). In this area, the seismic intensity is high. To ensure safe operation of the tunnel, it is necessary to investigate the mutual influence mechanism between the soft-soil interlayer and the shield tunnel under seismic conditions and guide seismic design.

With respect to soft soil seismic subsidence, the current focus is mostly on surface structures. Gu et al., (2019) conducted nonlinear dynamic finite element analysis of the seismic subsidence response at soft soil sites with upper structures via the OpenSees numerical simulation method and studied the impact of various factors on site settlement. Juan et al., (2020, 2024) studied the system response of soft soil, underground tunnels, and aboveground structures under seismic action, where the tunnel position affects the dynamic response of aboveground structures. Zhang et al., (2023) considered the influence of subway stations on the dynamic response of steel frame structures on soft soil layers and used

* Corresponding author. State Key Laboratory of Subtropical Building and Urban Science, School of Civil Engineering and Transportation, South China University of Technology, Guangzhou, 510640, China.
E-mail address: dqsong@scut.edu.cn (D. Song).
Peer review under the responsibility of Editorial Board of Earthquake Research Advances.

https://doi.org/10.1016/j.eqrea.2025.100393
Received 20 January 2025; Received in revised form 30 March 2025; Accepted 8 May 2025

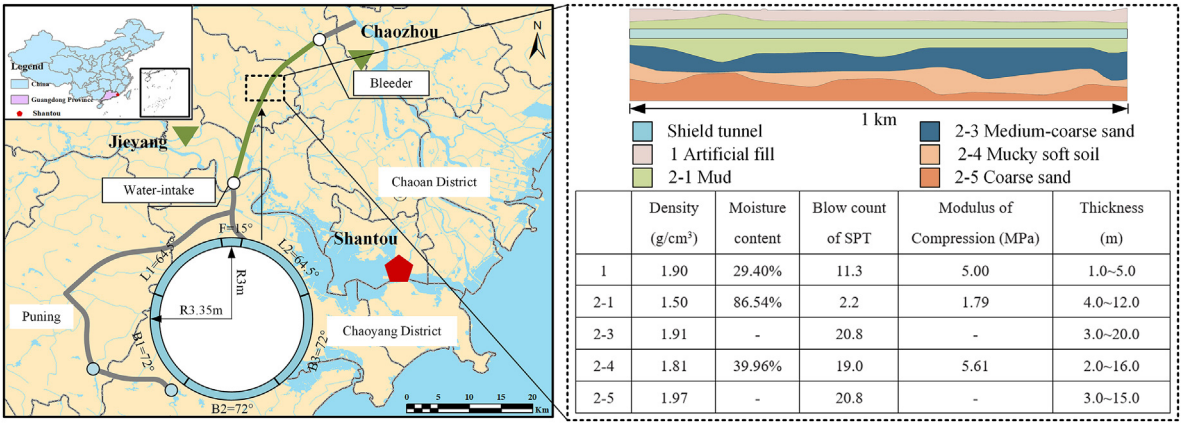

	Density (g/cm^3)	Moisture content	Blow count of SPT	Modulus of Compression (MPa)	Thickness (m)
1	1.90	29.40%	11.3	5.00	1.0~5.0
2-1	1.50	86.54%	2.2	1.79	4.0~12.0
2-3	1.91	-	20.8	-	3.0~20.0
2-4	1.81	39.96%	19.0	5.61	2.0~16.0
2-5	1.97	-	20.8	-	3.0~15.0

Fig. 1. Water conservancy project in the Chaoshan area.

ABAQUS software to establish a model, with the results indicating that the presence of subway stations leads to seismic wave reflection and refraction, thereby increasing the seismic response. Wang et al., (2021) established a method for analysing soft soil settlement of raft shallow foundations on the basis of the FLAC3D finite difference analysis platform and vibration softening model and investigated the influence of cylindrical underground structures within soft soil sites on shallow raft foundation seismic subsidence. In the study of soft soil–underground structures, the focus is on the structural response, with experiments and numerical simulations being common methods. He et al., (2024) studied the seismic response of shallow rectangular tunnels passing through saturated sandy and soft clay soils via centrifuge tests. Amith and Kumar, (2024) used a 1 g shaking table test to explore the interaction between tunnels and soil under dynamic loading. Zhang et al., (2024) conducted shaking table model tests to study the seismic response of pile foundations on inclined soft clay ground. Yan et al., (2025) compared and analysed the seismic response of underground structures at cohesive soil sites, liquefiable interlayer sites, and fully liquefied sites via centrifuge shaking table model tests. Huang et al., (2009) conducted centrifuge shaking table tests on large–scale piles–containing underground structures under seismic action to study their dynamic response characteristics, site settlement, and structural uplift. Chen et al., (2016) conducted shaking table model tests on subway stations in weak powdery clay sites under near- and far–field strong seismic motions, observing low–frequency amplification and high–frequency reduction of seismic waves in soft soil propagation. Jiang et al., (2024) established a three–dimensional numerical model of underground bifurcated tunnels in soft soil layers and analysed the seismic response characteristics and extent of tunnel damage. Gong et al., (2019) established a 2D stratum–tunnel model via ABAQUS finite element software and studied the seismic response of complex soft soil shield tunnels, paying a special attention to the arch bottom and arch waist regions under seismic action. Pham et al., (2024) studied the dynamic response of circular, rectangular and near-rectangular tunnels under seismic loads and reported that the seismic performance of tunnels of different shapes differed. Huang et al., (2020) evaluated the vulnerability of tunnels in Shanghai's soft soil via numerical simulations. Li et al., (2019) conducted numerical calculations of soft soil seismic settlement in subway tunnels via ABAQUS finite element software and softening modulus theory, which revealed that the presence of tunnel structures increases soil settlement values. When studying the seismic response of soil–underground structures, conducting shaking table tests is costly and time–consuming, making numerical simulation methods more common. However, some constitutive models do not accurately describe the dynamic behavior of soft soil. Centrifuge tests revealed that the PM4Silt constitutive model in Flac performs well in simulating the response of shallow soft soil but poorly for deep soft soil responses (Mohammad et al., 2024). The equivalent linear method is commonly used in simulating soft soil, with Liang et al., (2017) employing the equivalent linear method to simulate the nonlinear characteristics of soil and establishing a 3D nonlinear seismic response analysis model for deep thick soft soil overlying elastic bedrock. Milind et al., (2018) used finite element methods to establish simple structural models and analysed the seismic response and influencing factors of tunnels in soft soil layers. Lee et al., (2020) analysed the effects of horizontal loads on pile foundations in soft soil layers during earthquakes through centrifuge tests and numerical simulations and studied responses such as pile bending moments. From the above studies, it is evident that there are some issues in current numerical research, i.e., the limited research on the interaction mechanisms between soft soil interlayers and structures, the insufficiently detailed structural models, and the incomplete simulations of soft soil settlement characteristics. Furthermore, under general stratum conditions, shield tunnels are prone to severe damage under seismic action (Kazuhide et al., 2007; Athanasios et al., 2024; Katariwala et al., 2024), with significant seismic responses in liquefied sandy soil tunnels (Shen et al., 2024; Xu et al., 2024), indicating that shield tunnels in easily collapsible soft soil sites can be highly dangerous.

In this paper, based on the follow-up optimization project for the Hanjiang, Rongjiang, and Lianjiang water system connections, the interaction mechanism between soft soil and shield tunnels is analysed by treating the shield tunnel as the object and soft soil subsidence as the problem. The dynamic properties of soft soil are explored via dynamic triaxial tests. The PIMY constitutive model was used to characterize the settlement behavior of soft soil, and a refined finite element model was established via the open–source software framework OpenSees. The dynamic responses of the soil and structures under conditions with and without soft soil interlayers were studied, and the dynamic mutual influence mechanism between the soft soil and tunnel was analysed, providing a reference for the construction of shield tunnels in soft soil layers.

2. Dynamic characteristics of soft soil

The residual strain theory (Yu and Shi, 1989) can provide a preliminary explanation for soft soil seismic subsidence. The reasons for settlement are quite complex and can be summarized as structural effects, inertial effects, softening effects, and soil reconsolidation deformation. During an earthquake, the cement material in the soil is destroyed, the pore water pressure increases, and the soil skeleton tends to shrink. To investigate the dynamic properties of soft soil, samples of the 2–1 soil layer were taken, and dynamic triaxial tests were conducted. The test procedures included sample installation, sample saturation and consolidation, sample loading, and data recording and processing, with some experimental processes shown in Fig. 2. The confining pressure was

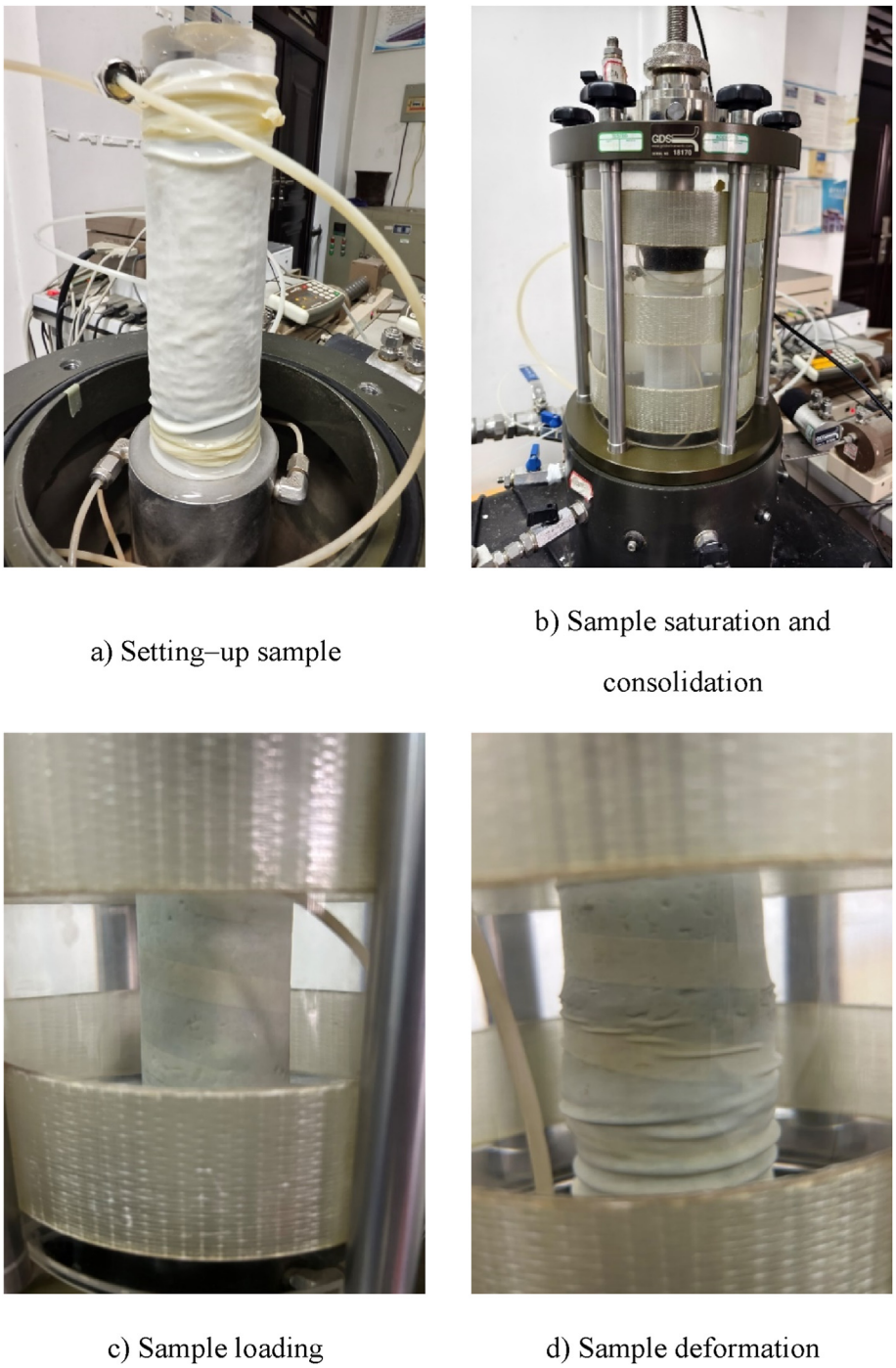

Fig. 2. Partial test procedure.

designed on the basis of the burial depth of the soft soil, and dynamic modulus tests and dynamic strength tests were conducted following the above steps to obtain the corresponding results.

2.1. Tests for determining the dynamic modulus of soils

The dynamic modulus test adopts step-by-step loading to apply seismic waves. The test scheme is shown in Table 1.

The nonlinear stress–strain behavior of soil is typically represented via a hyperbolic model, where the reciprocal of the dynamic elastic modulus is linearly related to the dynamic strain, as expressed in Eq. (1). The dynamic modulus test results are shown in Fig. 3.

Table 1
Dynamic modulus test scheme.

	Confined pressure (kPa)	Axial dynamic stress (kPa)		
		Initial value	Increment	End value
Case1	50	10	5	30
Case2	100	10	10	50
Case3	150	20	10	60

$$\frac{1}{E_d} = \frac{\varepsilon_d}{\sigma_d} = a + b\varepsilon_d \tag{1}$$

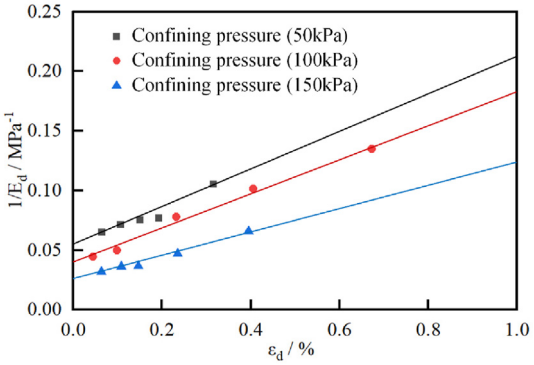

Fig. 3. $1/E_d \sim \varepsilon_d$ relationship for samples.

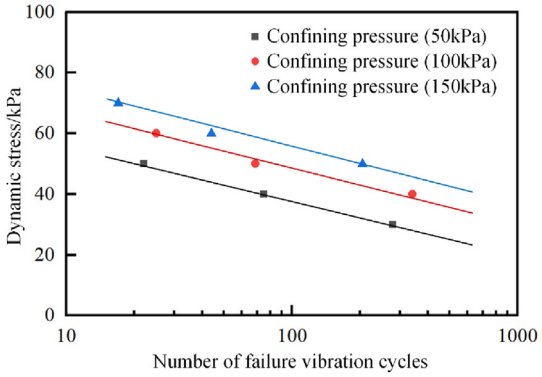

Fig. 4. Dynamic stress vs. number of failure vibration cycles.

where a and b are parameters obtained by the experiment, E_d is the dynamic elasticity modulus, and ε_d is the dynamic strain.

Fig. 3 shows that under the same conditions, as dynamic strain increases, the dynamic elastic modulus gradually decreases, indicating the softening effect of the soil under dynamic loading. With increasing confining pressure, the dynamic elastic modulus also increases. This means that soft soils with better structural integrity exhibit greater resistance to deformation, indicating that soft soils with better structures are less susceptible to seismic subsidence.

Since the unit weight of the 2–1 soil layer is 15 kN/m^3 and the burial depth is mostly more than 5 m, the maximum dynamic elastic modulus of the soft soil is taken as the average of the values at confining pressures of 100 kPa and 150 kPa, which is 34 MPa. Therefore, the maximum dynamic shear modulus of the soil can be calculated as 12.1 MPa.

2.2. Tests for determining the dynamic strength of soils

The dynamic strength test uses a single-stage loading method to apply seismic waves. The test scheme is shown in Table 2.

In the dynamic strength test, when the strain reached 5%, the sample failed. From this, the relationship curve between the failure dynamic stress and the corresponding failure vibration cycles under different confining pressures can be obtained. This curve can be plotted in a semilogarithmic coordinate system, as shown in Fig. 4.

From Fig. 4, in a semilogarithmic coordinate system, the relationship between the dynamic stress and failure vibration cycles generally shows a linear trend. As the dynamic stress increases, the sample requires fewer vibration cycles to reach failure. This indicates that under seismic conditions, the greater the inertial forces in the soil are, the more susceptible it is to seismic subsidence. Additionally, under the same conditions of failure vibration cycles, as the confining pressure increases, the dynamic stress required for the sample to reach failure also increases. This implies that soft soils with better consolidation exhibit greater resistance to failure. In other words, well–structured soft soils are more resistant to seismic subsidence.

Table 2
Dynamic strength test scheme.

	Confined pressure (kPa)	Axial dynamic stress (kPa)
Case 1	50	30
Case 2	50	40
Case 3	50	50
Case 4	100	40
Case 5	100	50
Case 6	100	60
Case 7	150	50
Case 8	150	60
Case 9	150	70

3. Constitutive model of soft soil and numerical model construction

This research needs a fine-grained soft soil constitutive model, which is complex and inefficient to develop in Abaqus or Ansys. Opensees is a computing platform specifically used for seismic analysis, which is more suitable for the research problem in this study. This study is based on OpenSees platform research.

3.1. Model characterization of soft soil

The PIMY constitutive model is capable of effectively simulating the settlement behavior of soft soil (Poudel and Chaulagain, 2024; Ozturk et al., 2024). In this model, the yield function is defined as a cylindrical multi–surface with the yield surface type being the Von Mises yield surface. The equation for the yield surface is shown in Eq. (2). In the equation, bold letters represent tensors, and ':' denotes the double dot product operation between tensors.

$$f = \left\{\frac{3}{2}((\boldsymbol{s}-\boldsymbol{\alpha}):(\boldsymbol{s}-\boldsymbol{\alpha}))\right\}^{\frac{1}{2}} - K = 0 \tag{2}$$

where f is a functional symbol, $\boldsymbol{s}$ is the deviatoric stress tensor, $\boldsymbol{\alpha}$ is the back stress tensor, and K is a parameter for defining the yield surface size.

The individual yield equation defines a cylindrical yield surface in the principal stress space, which appears as a circle on the deviatoric plane. By applying the multiple yield surface theory, stacked yield surfaces can be obtained, as illustrated in Fig. 5.

The shear stress and shear strain in this model are related through the shear modulus, as shown in Eq. (3), and the shear stress–strain curve is

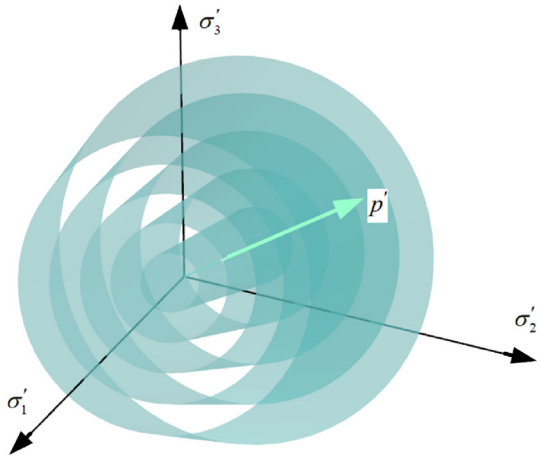

Fig. 5. Criterion of multiple yield surfaces in the principal stress space.

depicted in Fig. 6. This model employs an associated flow rule, which posits that the increment of plastic strain is orthogonal to the yield surface. Additionally, it utilizes the incremental plasticity theory, which requires the sizes of multiple yield surfaces to remain constant, with only their positions changing.

$$\tau_{oct} = \frac{G_{\max}\gamma_{\mathrm{oct}}}{1+\frac{\gamma_{\mathrm{oct}}}{\gamma_r}} \tag{3}$$

where τ_{oct} is the octahedral shear stress, $\tau_{\mathrm{oct}} = \frac{1}{\sqrt{3}}\sqrt{s:s}$, $G_{\max}$ is the shear modulus at low strain, γ_{oct} is the octahedral shear strain, and γ_{r} is the internally calculated shear strain used to define the shape of the curve, $\gamma_{\mathrm{r}} = \frac{\gamma_{\max}\tau_{\max}}{G_{\max}\gamma_{\max}-\tau_{\max}}$, where $\tau_{\max}$ corresponds to the shear strength associated with the peak shear strain $\gamma_{\max}$.

Implementing the PIMY model in OpenSees involves several steps. First, parameter initialization, where the shape and size of the yield surfaces are constructed based on the input material parameters. Next, the stress update algorithm is used to solve for stress. This involves providing initial strain and initial stress, specifying strain increments, and using the constitutive equations to calculate stress increments, ultimately obtaining the stress. Subsequently, it is necessary to check if the stress and strain comply with the model's requirements; if not, stress correction is needed. Finally, the correct stress and strain values are output. The operational flow of this material model is illustrated in Fig. 7.

During stress calculations, OpenSees uses explicit integration algorithms, which divide the predefined strain increments into several subincrements for computation, as shown in Eq. (4). Additionally, when calculating stress, it is necessary to compute the shear modulus of the material, which is dependent on the position of the material within multiple yield surfaces at that moment.

$$\Delta\sigma_n^k = \frac{1}{m}\sum_{j=0}^{m-1} \boldsymbol{D}_{n+j/m}^{\mathrm{ep}}\Delta\varepsilon_n^k \tag{4}$$

where $\Delta\sigma_n^k$ is the stress increment, m is the number of subincrements, $\boldsymbol{D}_{n+j/m}^{\mathrm{ep}}$ is the tangent elastoplastic matrix calculated on the basis of the new stress and state variables obtained from the previous strain subincrements, and $\Delta\varepsilon_n^k$ is the strain increment.

3.2. Finite element model

Based on the design data, a two–dimensional finite element model was established via the 'soil–structure' method on the OpenSees platform, as shown in Fig. 8. The inner diameter of the shield tunnel was 6 m, the outer diameter was 6.7 m, and the burial depth was 10.65 m. The tunnel lining consisted of one crown block, two adjacent blocks, and three standard blocks.

Considering the influence of boundary effects, the distance between the transverse boundary where the tunnel intersects with the soil is approximately 8 times the width of the tunnel outer diameter, whereas the distance between the bottom boundary where the tunnel intersects with the soil is approximately 5 times the width of the tunnel outer diameter. The lateral length of the soil was 100 m, the vertical height was 50 m, the thickness of the soft soil layer was 8 m, and the middle of the soft soil layer was aligned with the center of the tunnel. The mesh around the tunnel and the surrounding soil was dense and small, whereas the mesh farther away was sparse and larger. The main body of the tunnel lining and joints were simulated via four–node quadrilateral elements, and the bolts were simulated via truss elements. To account for the fluid–structure coupling effect, the soil at the site was modelled via four–node fluid–solid coupling elements on the basis of the U–P format of the Biot theory. This model consisted of 9 832 nodes and 9 446 elements.

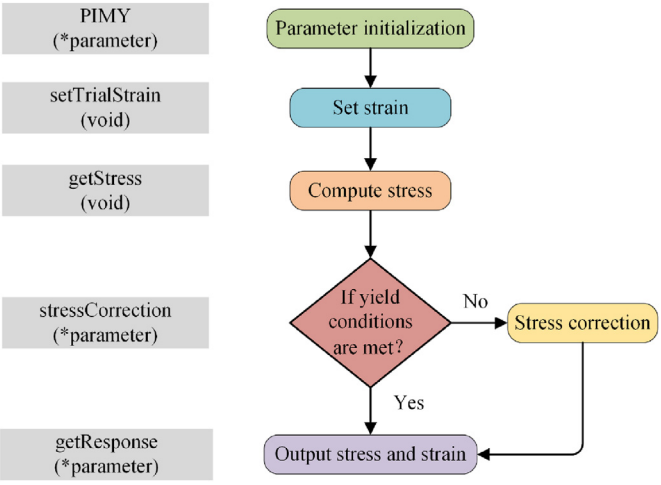

Fig. 7. Implementation process and internal functions of the PIMY.

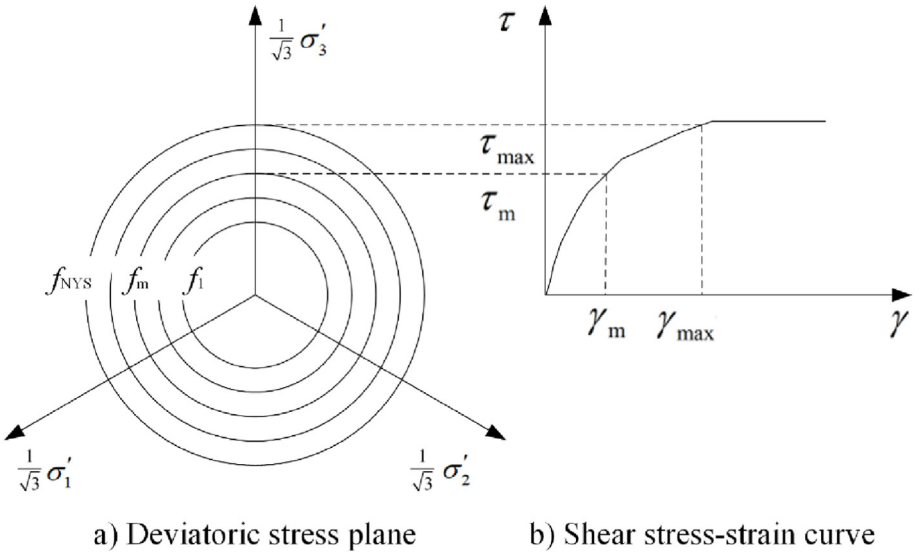

Fig. 6. PIMY shear stress–strain relationship.

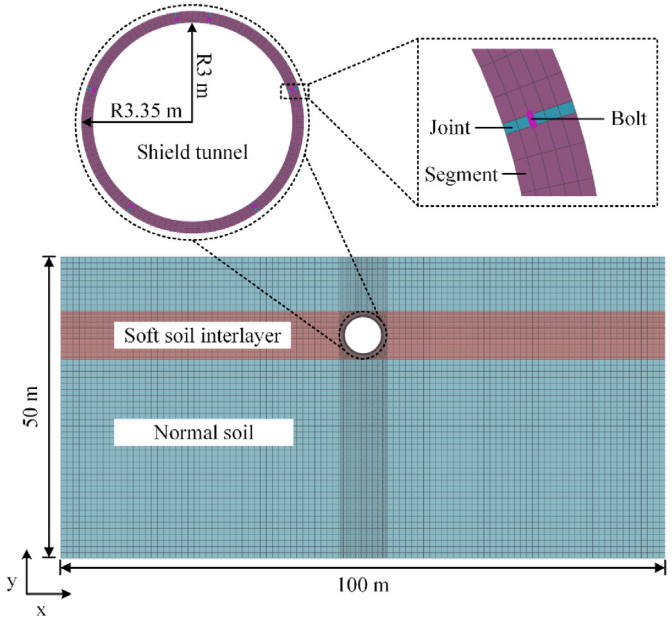

Fig. 8. Finite element model.

3.3. Material constitutive model and parameters

The numerical model includes the shield tunnel and the surrounding soil. Next, we introduce their constitutive models and material parameters separately. In this study, based on the different materials, the shield tunnel was divided into segments, joints, and bolts, with the relevant parameter values shown in Table 3. The main body of the segment was composed of steel bars and C55 concrete, which generally has a high stiffness and is not easily damaged. Therefore, a linear elastic constitutive model was used to simulate it. For joints, the presence of segment segmentation and bolt holes reduces the concrete's deformation resistance at the joint. Therefore, a stiffness-reduction method was applied to simulate the concrete at the joint, with the elastic modulus reduced to 3% and the yield stress reduced to 50%. Additionally, the tension–compression behavior at the joint was significantly different. Hence, a modified Mohr–Coulomb elastoplastic constitutive model, specifically the Drucker–Prager elastoplastic constitutive model, was used to simulate the joint. To account for the different tension–compression stiffnesses, an elastic material only under compression was added at the joint. The bolts were made of steel and were simulated via the Giuffre–Menegotto–Pinto constitutive model. The soil can be divided into a soft soil interlayer and other soil layers, both of which are simulated via the PIMY constitutive model. The soft soil interlayers used the parameters of layer 2–1, whereas the other soil layers used normal soil layer parameters.

3.4. Boundary and load conditions

The boundary conditions of the model included fixed constraints at the bottom, which restrained the lateral and vertical displacements of the bottom soil. Periodic boundaries were applied on the sides, meaning that points at the same height on the left and right sides had the same lateral and vertical displacements. Based on the hydrogeological conditions, the groundwater level was assumed to reach the ground surface, and the pore water at the top of the model was constrained. The top of the model was treated as a free-drainage surface, whereas the lateral and bottom boundaries were impermeable.

Seismic loading was applied at the bottom of the tunnel in the form of horizontal acceleration. Given that the maximum seismic intensity in the Chaoshan region could reach level VIII and that the El–Centro wave is a classic natural wave with a broad spectrum of components used in seismic analysis, an El–Centro wave with an amplitude of 0.2 g was applied for loading. The acceleration time history curve of this wave is shown in Fig. 9.

4. The mutual influence mechanism of soft soil–tunnels

To investigate the mutual interaction mechanism between soft soil and tunnels, this section presents calculations of the seismic response of the soil and structures with and without a soft soil layer, revealing certain patterns.

4.1. Soil responses

The soil responses encompass the acceleration, displacement, excess pore pressure ratio, and shear stress–strain variations of the soil. The observation and analysis points for the soil near and far from the tunnel were selected, as shown in Fig. 10.

The acceleration responses at various locations with and without a soft soil layer are shown in Fig. 11. A comparison of the peak accelerations at points A and B1 with and without a soft soil layer clearly reveals that the presence of the soft soil layer increases the acceleration peak values of the soil layer where the tunnel is located. A comparison of the variations in the acceleration peak values at points B1, B2, and B3 reveals that the peak acceleration values exhibit an amplification effect in the general soil layers, whereas they rapidly attenuate within the soft soil layer.

The soil response patterns differ when a soft soil layer is present or absent. The focus here is on the soil response in the presence of a soft soil

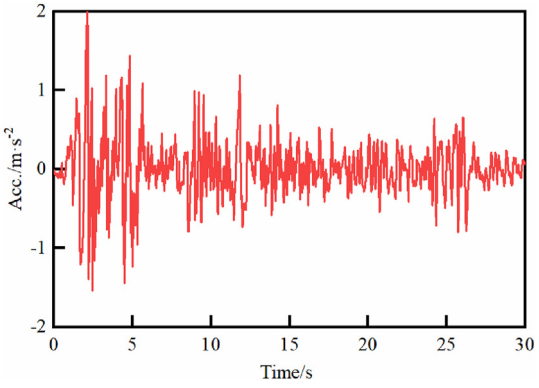

Fig. 9. Acceleration time history curve of the El–Centro wave.

Table 3
Material parameters.

	Density (kg/m^3)	Elasticity modulus (MPa)	Maximum shear modulus (MPa)	Maximum bulk modulus (MPa)	Poisson's ratio	Yield stress (MPa)
Segment	2 400	3.55×10^4	–	–	0.167	–
Joint	2 400	1.07×10^3	–	–	0.167	17.75
Bolt	7 850	2.06×10^5	–	–	0.3	640
2–1 layer	1 500	–	12.5	58.3	–	–
Normal soil layer	1 800	–	15.0	75.0	–	–

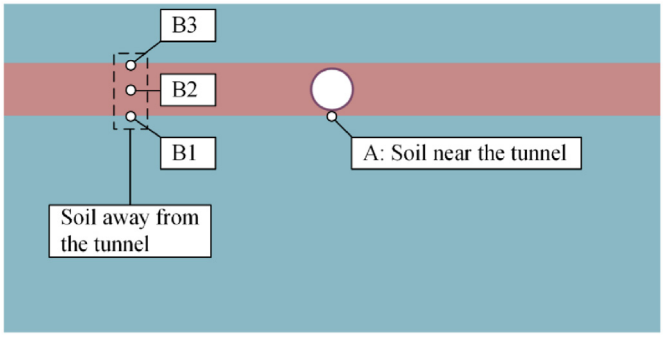

Fig. 10. Soil observation and analysis points.

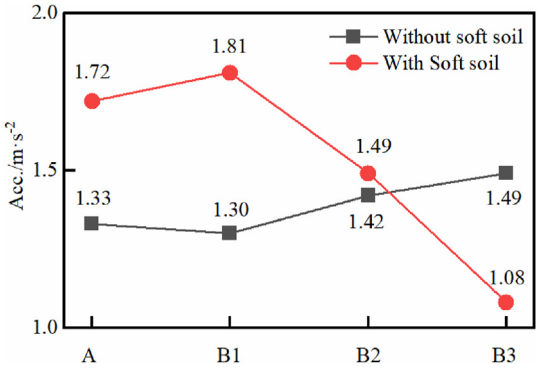

Fig. 11. Peak accelerations at various locations with and without a soft soil layer.

layer. The Fourier spectra of the El–Centro wave and the acceleration at point B3 are shown in Fig. 12. In the presence of a soft soil layer, the high–frequency components of seismic motion decrease underground, whereas the low–frequency components are significantly amplified.

The displacement response of the near–field and far–field soils due to seismic motion (taking B1 as an example) is shown in Fig. 13. The *x*–direction displacement curves of the soil at both locations are similar, following a trend consistent with the integration of the input acceleration at the base, and both exhibit a certain amount of lateral displacement at the end of the seismic motion. There is a significant difference in the *y*–direction displacement of the soil at the two locations. Under seismic action, the near–field soil continuously subsides, with the rate of subsidence gradually slowing, resulting in a final settlement of 0.57 cm. The vertical displacement of the far–field soil remains relatively stable, initially decreasing and then increasing, with a final uplift of 0.03 cm. The above results indicate that under seismic action, the soil near the tunnel structure experiences settlement, whereas the soil further experiences uplift due to the subsidence of the intermediate soil.

The pore pressure ratio response of the near–field and far–field soils is shown in Fig. 14. The pore pressure ratio of the soil at both locations undergoes significant changes in the first few seconds, after which it stabilizes around a certain level with some fluctuations. The pore pressure ratios in the soil are relatively low, consistent with the characteristics of soft soil. The pore pressure ratio at location A is greater than that at B1, and the pore pressure in the soil at location A exhibits noticeable fluctuations during the accumulation process. This is likely due to its proximity to the structure.

The shear stress–shear strain responses of the near–field and far–field soils are shown in Fig. 15. The shear stress–shear strain curves of the soil exhibit hysteresis behavior, reflecting the material properties of the soil. Furthermore, the shear strain in the soil located near the tunnel is greater than that in the soil farther from the tunnel. This indicates that the soil near the tunnel experiences enhanced shear effects.

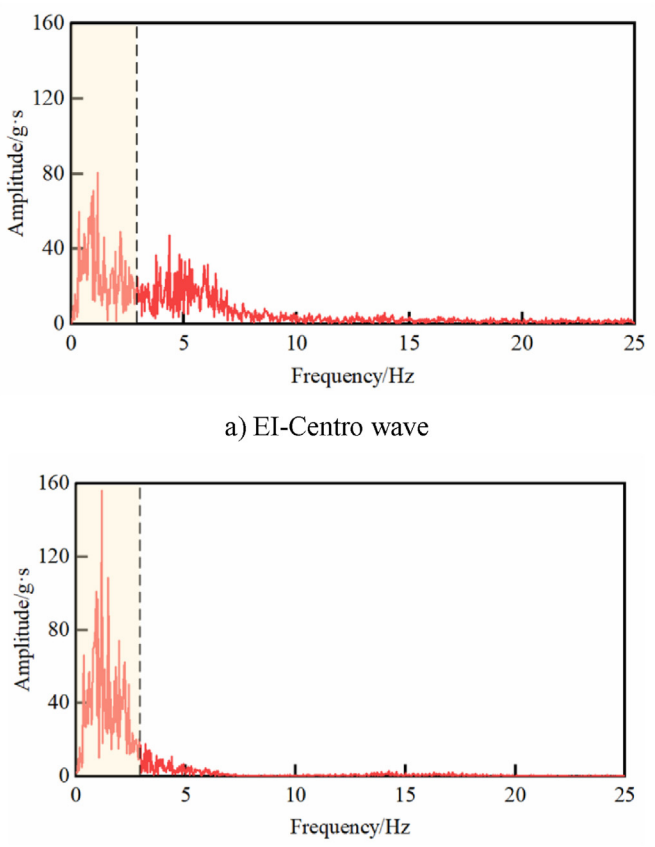

Fig. 12. Fourier spectra of the input wave and measurement point.

4.2. *Responses of the structure*

The responses of the structure are reflected by changes in the tunnel inclination angle, displacement, bolt stress, and joint opening, as shown in Fig. 16.

The responses of the tunnel inclination angle with and without a soft soil layer are shown in Fig. 17. The tunnel inclination angle exhibits severe fluctuations during the seismic process, indicating that the shape of the tunnel is constantly changing. In the presence of a soft soil layer, the tunnel inclination increases significantly, reaching a maximum ofincreases significantly, reaching a maximum of 0.256%.

The tunnel displacement is obtained by averaging the displacement values at four points inside the tunnel: top, bottom, left, and right. The displacement response is shown in Fig. 18. The *x*–direction displacement of the tunnel is consistent with the displacement curve obtained by integrating the bottom input acceleration with respect to time. When a soft soil interlayer is present, the tunnel's lateral displacement is greater. In both cases, the *y*–direction displacement of the tunnel rapidly increases at the beginning of the vibration and continues to increase with time, albeit at a decreasing rate. This indicates that the tunnel experienced seismic subsidence. With a soft soil interlayer, the tunnel's settlement displacement is much greater, reaching a maximum of 0.787 cm.

The bolt stresses and joint opening responses are shown in Fig. 19. With a soft soil interlayer, the bolt stresses and joint opening displacements at various positions are significantly greater than those in the case without a soft soil interlayer. In the presence of a soft soil interlayer, the maximum values of bolt stress and joint opening occur at bolt5 and joint5, respectively. The maximum bolt stress is 344 MPa, and the maximum joint opening displacement is 0.835 mm.

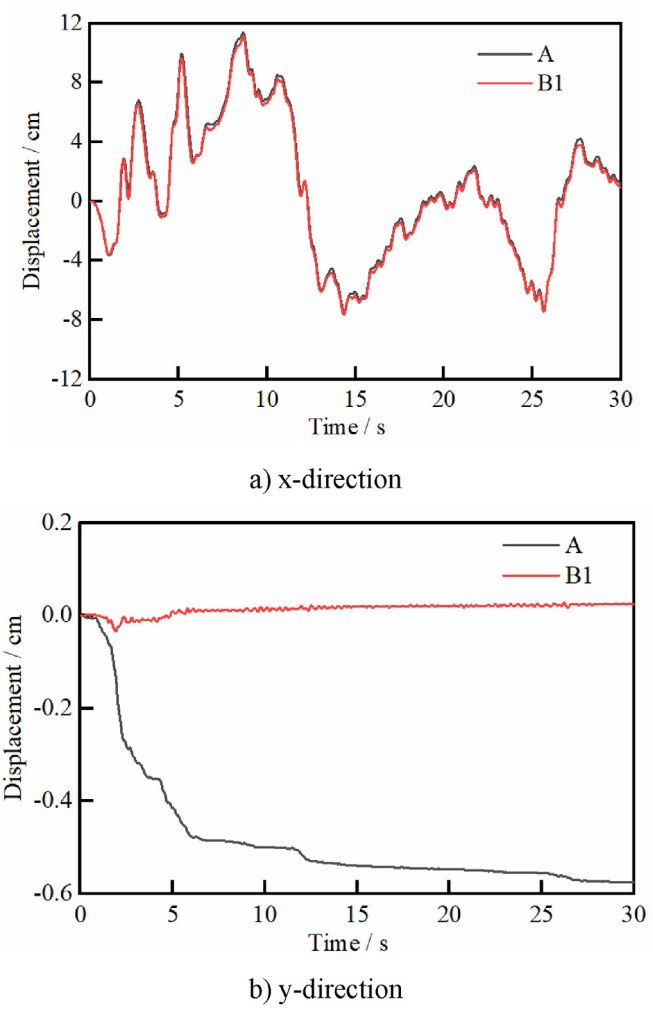

Fig. 13. Displacement response in different directions.

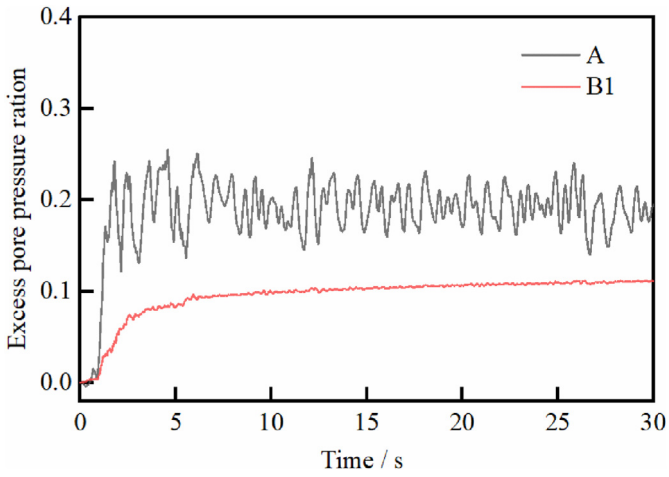

Fig. 14. Excess pore pressure response.

4.3. Discussion and analysis

Based on the above dynamic response results, the mutual influence mechanism between the soft soil interlayer and the shield tunnel can be identified. First, the presence of the shield tunnel exacerbates the settlement of the soft soil. On the one hand, under seismic action, the surrounding soil around the tunnel experiences significant inertial forces from the tunnel structure, increasing soil stress and accelerating its softening. This is manifested by a stronger shear effect on the soil near the tunnel, resulting in larger settlement displacements. On the other hand, the presence of the tunnel impedes soil drainage, accelerating the accumulation of pore water pressure, leading to a significant decrease in effective stress and increased soil deformation. This is manifested by a rapid increase in pore water pressure in the soil surrounding the tunnel. When summarizing the research progress on structural aseismic resistance under soft soil foundations, Cheng et al., (2024) reached the same conclusion. Under the action of an earthquake, excessive pore pressure in the soil mass results in destruction of part of the soil skeleton and a reduction in the shear strength and stiffness of the softened soil mass,

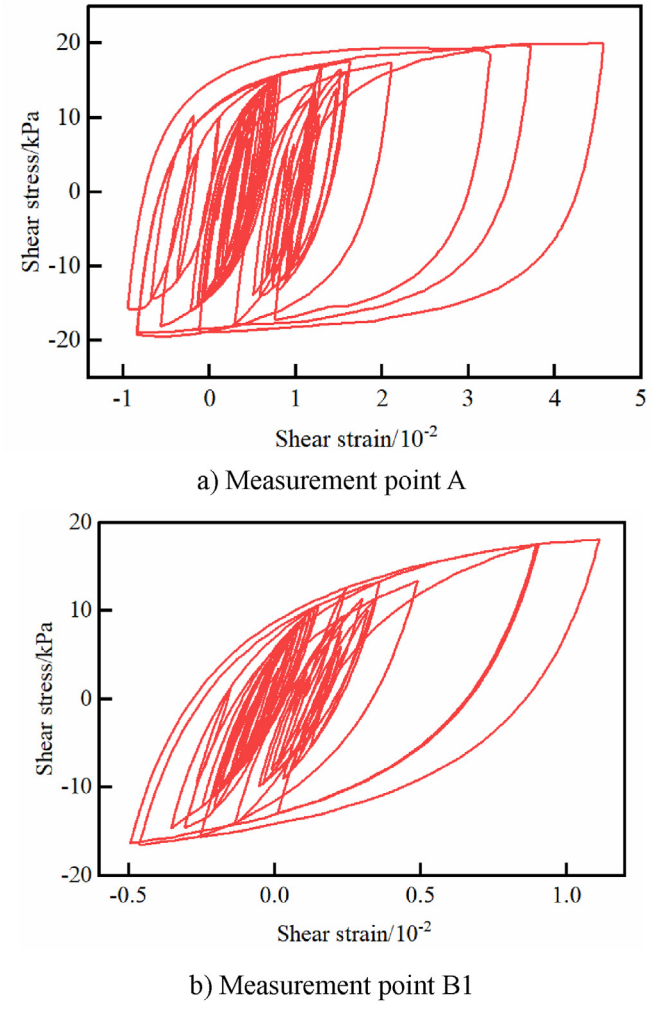

Fig. 15. Shear stress–shear strain response at A and B1.

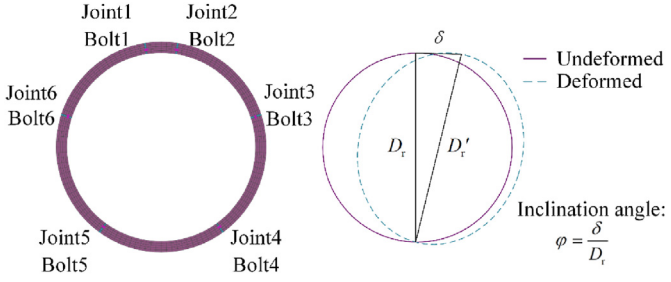

Fig. 16. Observation positions and indices of the tunnel.

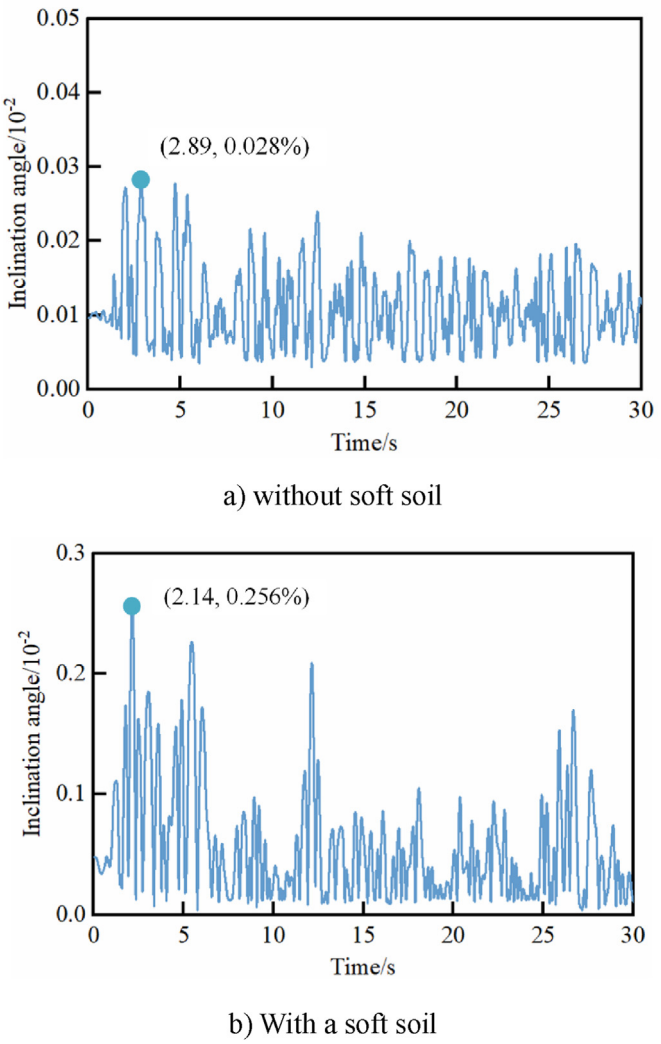

Fig. 17. Curve of tunnel inclination.

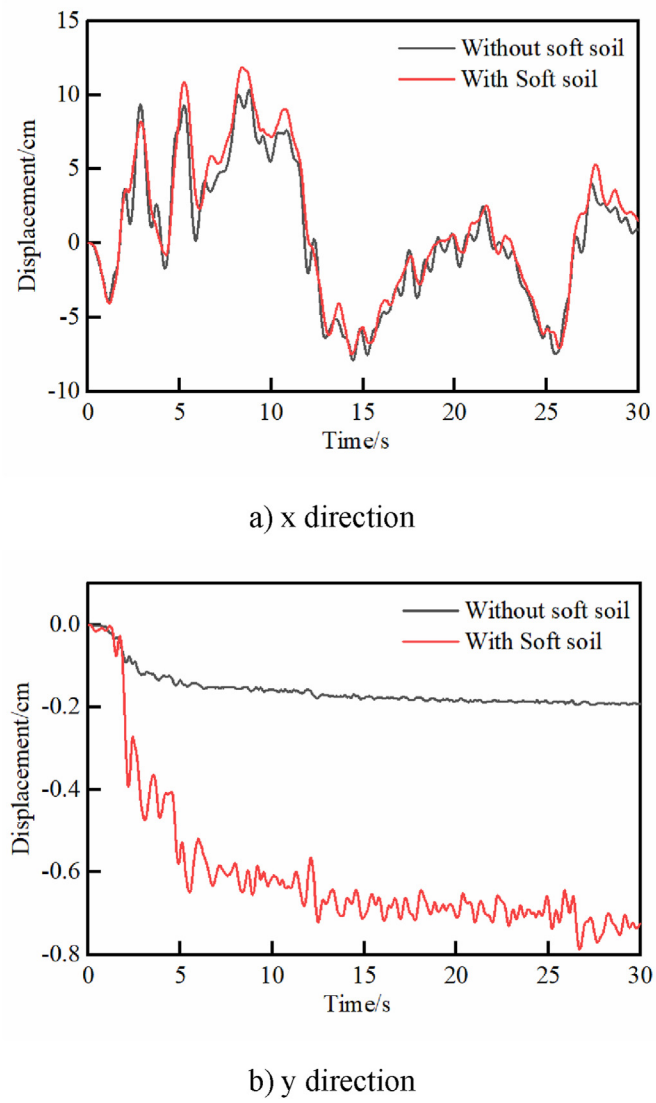

Fig. 18. Displacement of the the tunnel.

thus weakening the overall strength and stiffness of the soil mass.

Furthermore, under seismic action, the stress and deformation of the settling soft soil are significant, leading to substantial increases in the stress, deformation, and displacement of the structure, which is similar to the rule obtained by Sun et al., (2020). The dynamic action on the soft soil layer is stronger, as evidenced by the higher peak accelerations transmitted into this layer. This is due to the presence of a weak interface between the soft soil layer and the ordinary soil layer, where seismic waves are reflected and amplified. As seismic waves exit the soft soil layer, the peak acceleration decreases significantly, indicating that the soft soil layer absorbs a considerable amount of seismic energy. Furthermore, soft soil is more prone to deformation, which results in deformation and displacement in tunnels within soft soil. For example, settlement of the soft soil induces settlement of the tunnel, whereas shear deformations in the soft soil lead to shear deformations in the tunnel. Additionally, when there is a soft soil interlayer, the tunnel experiences significant bolt stress and joint opening, with bolt4 and bolt5 and joint4 and joint5 showing notably greater responses than other locations. This finding indicates that under seismic action, the arch foot position is most susceptible to damage in the tunnel.

5. Conclusions

On the basis of an analysis combining experimental and numerical methods on the dynamic influence mechanism between soft soil and shield tunnels, the following conclusions have been drawn.

(1) The dynamic characteristics of soft soil are studied via dynamic triaxial tests, and the calculation parameters of soft soil are obtained. Dynamic modulus and dynamic strength tests show that soil deforms and softens under dynamic loading. The better the structure of soft soil is, the less earthquake subsidence occurs. Earthquake subsidence is more likely to occur when soft soil is subjected to greater inertia forces.

(2) The presence of the shield tunnel exacerbates the settlement of the soft soil, as the surrounding soil experiences significant inertial forces from the tunnel structure, hindering drainage and accelerating the accumulation of pore water pressure.

(3) The soft soil itself experiences large deformation and displacement under the action of earthquakes, which leads to high stress, deformation, and structural displacement. The arch foot position of the tunnel is identified as the most vulnerable to damage.

(4) Soft soil interlayers should be avoided in the design and construction of shield tunnels, and antivibration measures should be taken when passing through soft soil interlayers is unavoidable.

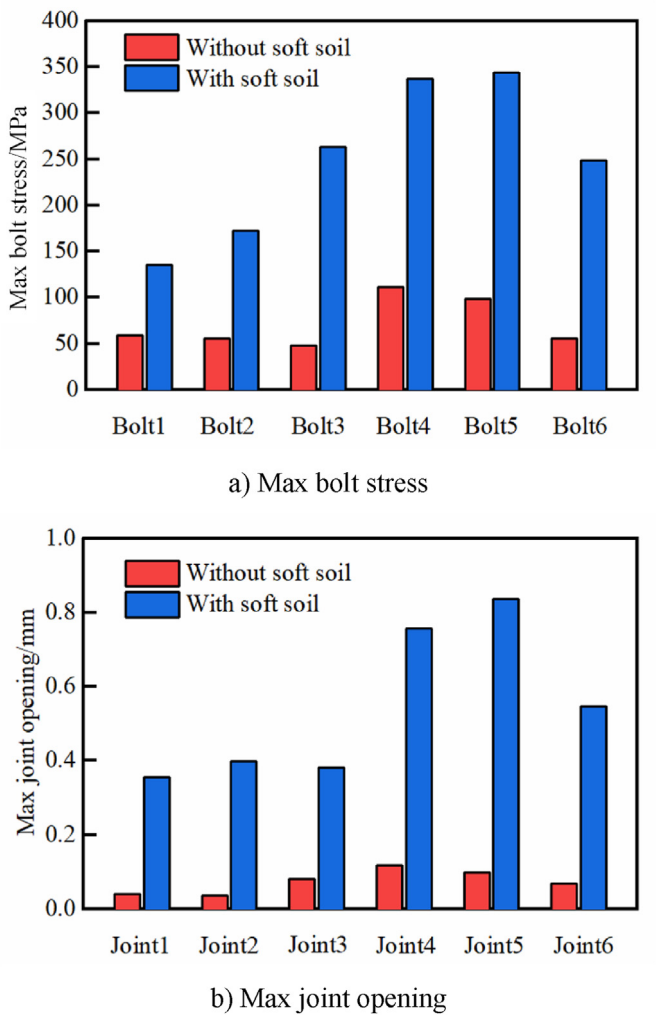

Fig. 19. Responses of the bolts and joints.

CRediT authorship contribution statement

Xinwei Tang: Writing – review & editing, Visualization, Validation, Supervision, Project administration, Methodology, Funding acquisition, Conceptualization. **Gaozhi Xin:** Writing – original draft, Visualization, Software, Investigation. **Danqing Song:** Writing – review & editing, Visualization, Validation, Supervision, Methodology, Funding acquisition, Conceptualization.

Declaration of competing interest

The authors declare that they have no known competing financial interests or personal relationships that could have appeared to influence the work reported in this paper.

Author agreement and acknowledgement

This work was funded by the Key Research and Development Projects of Guangdong Province (2019B111108001), China and the Guangdong Basic and Applied Basic Research Foundation (2024A1515010045), China and the Basic Research Program of Jiangsu (BK20231217 and BK20220265), the independent research project of the State Key Laboratory of Subtropical Building and Urban Science (2023ZB15), China the Key Laboratory of Geomechanics and Geotechnical Engineering Safety, the Chinese Academy of Sciences (SKLGME023001), China and the Open Research Fund Program of the State Key Laboratory of Hydroscience and Engineering (SKLGME-KF-2025-D-02), China. Appreciation is expressed to Assoc. Prof. Yichao Gao for their substantial support for the test data processing work of this work.

References

Amith, K.S., Ganesh Kumar, S., 2024. A state-of-the-art review on 1-g experimental investigations on tunnels subjected to dynamic loading conditions. Eur. J. Environ. Civil Eng. 28 (6), 1300–1331.
Athanasios, Agalianos, Dario, Kern, Ioannis, Anastasopoulos, 2024. Reverse fault rupture propagation through dense sand and interaction with a shallow RC tunnel. Jpn. Geotech. Soc. Spec. 10 (20), 715–718.
Burak, Ozturk, Ahmed Fouad, Hussein, M., Hesham El Naggar, Hongjuan, Chen, 2024. Seismic response of a model soil–pile–bridge system in cohesive soil. Soil Dynam. Earthq. Eng. 187, 109013.
Chen, GuoXing, Chen, Su, Zuo, Xi, Qi, ChengZhi, Du, XiuLi, Wang, ZhiHua, 2016. Shaking table test on seismic response of subway station structure in soft ground. Rock Soil Mech. 37 (2), 331–342 (in Chinese).
Cheng, XueLei, Li, QiQi, Hai, Ran, Guo, ShouShou, Xing, XianFan, 2024. Research progress and prospects of seismic performance on underground structure embedded in soft soil foundation. Sci. Rep. 14 (1), 21883.
Gu, JunRu, Li, Ping, Tian, ZhaoYang, Zhou, ChunShu, Zhang, Yuan, 2019. Influence of ground motions on seismic subsidence of soft soil based on OpenSees. China Earthq. Eng. J. 41 (5), 1339–1346 (in Chinese).
Gong, GuoDong, Liang, JianWen, Ba, ZhenNing, Xu, AnQuan, Yan, QiChao, Wang, ZhiKai, 2019. Seismic transverse time–history analysis of shield tunneling complex soft soil. J. Tianjin Univ. 52 (S1), 106–112 (in Chinese).
He, ZhengYao, Nicolas G.L.H., Lee, Gopal Madabhushi, S.P., 2024. Seismic behaviour of shallow cut–and–cover tunnels. Jpn. Geotech. Soc. Spec. 10 (60), 2469–2473.
Huang, MaoSong, Liu, Ming, Liu, YanHua, 2009. Anisotropic bounding surface model for saturated soft clay under cyclic loading. J. Hydraul. Eng. 40 (2), 188–193+200 (in Chinese).
Huang, ZhongKai, Kyriazis, Pitilakis, Grigorios, Tsinidis, Sotirios, Argyroudis, Zhang, DongMei, 2020. Seismic vulnerability of circular tunnels in soft soil deposits: the case of Shanghai metropolitan system. Tunn. Undergr. Space Technol. 98, 103341.
Jara, J.M., Florio, E., Olmos, B.A., 2023. Seismic evaluation and reliability index of soft story buildings on flexible soils by via old and current seismic regulations in Mexico. Eng. Struct. 286, 116048.
Juan, M., Mayoral, G., Mosqueda, 2020. Seismic interaction of tunnel–building systems on soft clay. Soil Dynam. Earthq. Eng. 139, 106419.
Juan, Manuel Mayoral, Simón, Tepalcapa, Simon, Tepalcapa, Mauricio, Pérez, 2024. Seismic performance of tunnel–building–urban bridge systems in soft clays. Jpn. Geotech. Soc. Spec. 10 (60), 2504–2509.
Jiang, JiaWei, Tao Ran, M., Hesham, El Naggar, Liu, Hen, Du, XiuLi, 2024. Seismic performance and vulnerability analysis for bifurcated tunnels in soft soil. Comput. Geotech. 167, 106065.
Kazuhide, Y., Yoshiyuki, K., Mitsuru, S., 2007. Historical earthquake damage to tunnels in Japan and case studies of railway tunnels in the 2004 Niigataken–Chuetsu earthquake. Quarterly Report of RTRI 48 (3), 136–141.
Katariwala, A., Desai, A., Shah, H., 2024. "Effect of Seismic Excitation on Underground Tunnel". In: International Conference on Vibration Problems. Springer, Singapore.
Kiyoshi, Yamashita, Junji, Hamada, Sadatomo, Onimaru, Masahiko, Higashino, 2012. Seismic behavior of piled raft with ground improvement supporting a base-isolated building on soft ground in Tokyo. Soils Found. 52 (5), 1000–1015.
Li, Man, Liang, JianWen, Ba, ZhenNing, Zhu, YuTong, Zhang, JiuQi, Zhang, Ping, 2019. Finite element analysis of seismic settlement of shield tunnel in soft soil. China Civ. Eng. J. 52 (S1), 240–247 (in Chinese).
Liang, JianWen, Liang, JiaLi, Zhang, Ji, Ba, ZhenNing, 2017. Nonlinear seismic response of 3D canyon in deep soft soils. Chin. J. Geotech. Eng. 39 (7), 1196–1205 (in Chinese).
Lee, J., Il–Wha, L., Yun, W.C.C., Mintaek, Y., 2020. Centrifuge and numerical simulation of pile supported slab track system behavior on soft soil under seismic loading. KSCE J. Civ. Eng. 24 (11), 3179–3188.
Mohammad, Khosravi, Sujanraj, Devkota, Ali, Khosravi, Kami, Mohammadi, 2024. Numerical simulation of lightly overconsolidated clay layers of low plasticity subjected to strong shaking. Jpn. Geotech. Soc. Spec. 10 (52), 1970–1975.
Milind, Patil Deepankar, Choudhury, P.G., Ranjithc, Zhao J., 2018. Behavior of shallow tunnel in soft soil under seismic conditions. Tunn. Undergr. Space Technol. 82, 30–38.
Nolaraj, Poudel, Hemchandra, Chaulagain, 2024. Numerical investigation of nonlinear soil–structure interaction effects on response of irregular RC buildings. Results Eng. 22, 102161.
Shen, Yiyao, M., Hesham El Naggar, Zhang, DongMei, Li, LiYun, Du, XiuLi, 2024. Seismic response characteristics of shield tunnel structures in liquefiable soils. Soil Dynam. Earthq. Eng. 182, 108701.
Sun, Hong, Wang, HaiLin, Wu, Gang, Ge, XiuRun, 2019. The mechanical properties of naturally deposited soft soil under true three-dimensional stress states. Geotech. Test. J. 42 (5), 1370–1383.
Sun, QiangQiang, Daniel, Dias, Luis Ribeiro e, Sousa, 2020. Soft soil layer-tunnel interaction under seismic loading. Tunn. Undergr. Space Technol. 98, 103329.
Tong, Fei, Yin, JianHua, Pei, HuaFu, 2012. Experimental study on complete consolidation behavior of Hong Kong marine deposits. Mar. Georesour. Geotechnol. 30 (4), 291–304.

Van Vi, Pham, Ngoc Anh, Do, Piotr, Osinski, Ngoc Thai, Do, Daniel, Dias, 2024. Study on the tunnel shape and soil-lining interaction influencing the lining behavior under seismic loading. Earthq. Eng. Eng. Vib. 23 (4), 845–862.
Wang, YunLong, Wang, Jing, Yuan, XiaoMin, Ma, JiaJun, 2021. Numerical investigation on the influence of underground tubular structure on seismic subsidence of shallow raft foundation in soft soil site. Rock Soil Mech. 42 (12), 3485–3495 (in Chinese).
Xu, LingYu, Xi, JuPing, Cai, Fei, Chen, WeiYun, Cheng, GuoXing, 2024. Dynamic response of subsea tunnel in liquefiable layered seabed under combined earthquake and wave action. Ocean Eng. 301, 117595.
Yan, GuanYu, Xu, ChengShun, Zhang, ZiHong, Wang, XueLai, Du, XiuLi, 2025. Series of centrifuge shaking table tests study on seismic response of subway station structures in soft soil sites. Undergr. Space 21, 232–251.
Yu, ShouSong, Shi, ZhaoJi, 1989. Experimental investigation of soil settlement due to earthquake. Chin. J. Geotech. Eng. 4, 35–44 (in Chinese).
Zhang, HaiYing, Lu, JinYu, Shu, HaiGang, Jiang, HaoRui, 2023. Seismic response of a steel frame considering the underground subway–soft soil–steel frame interaction. J. Build. Eng. 80, 108005.
Zhang, Lei, Hu, ZhengLing, Zhang, PanPan, Chen, Cheng, Rui, Rui, 2024. Seismic response of pile–cap system installed in inclined soft clayey ground. Soil Dynam. Earthq. Eng. 181, 108658.